J Biomol NMR (2007) 38:41–46
DOI 10.1007/s10858-006-9139-1

ARTICLE

Strong coupling effects during *X*-pulse CPMG experiments recorded on heteronuclear *ABX* spin systems: artifacts and a simple solution

Pramodh Vallurupalli · Lincoln Scott · James R. Williamson · Lewis E. Kay

Received: 30 November 2006 / Accepted: 18 December 2006 / Published online: 3 March 2007

Abstract Simulation and experiment have been used to establish that significant artifacts can be generated in *X*-pulse CPMG relaxation dispersion experiments recorded on heteronuclear *ABX* spin-systems, such as $^{13}C_i$–$^{13}C_j$–^{1}H, where $^{13}C_i$ and $^{13}C_j$ are strongly coupled. A qualitative explanation of the origin of these artifacts is presented along with a simple method to significantly reduce them. An application to the measurement of ^{1}H CPMG relaxation dispersion profiles in an HIV-2 TAR RNA molecule where all ribose sugars are protonated at the 2′ position, deuterated at all other sugar positions and ^{13}C labeled at all sugar carbons is presented to illustrate the problems that strong ^{13}C–^{13}C coupling introduces and a simple solution is proposed.

Keywords Strong scalar coupling · ^{1}H CPMG relaxation dispersion · Spin-lock · *ABX* heteronuclear spin-system · RNA

Introduction

Relaxation dispersion NMR spectroscopy has become a powerful tool for studying conformational dynamics of biomolecules on the μs–ms time-scale (Palmer 2004; Eisenmesser et al. 2005; Korzhnev et al. 2004; Ishima et al. 1998). For molecules undergoing ms dynamics, Carr–Purcell–Meiboom–Gill based experiments are particularly useful (Palmer 2004). Here the evolution of transverse magnetization under a series of refocusing 180° pulses is quantified to obtain information on the time-scale of the exchange process as well as on the population(s) and chemical shifts of the excited state(s). In addition, experiments can be repeated as a function of temperature or pressure to obtain insight into the energy landscape of the system (Bezsonova et al. 2006; Korzhnev et al. 2004). A variety of CPMG-based experiments have been developed for the study of exchange in proteins, including those that make use of ^{1}H, ^{13}C and ^{15}N nuclei (Ishima and Torchia 2003; Orekhov et al. 2004; Loria et al. 1999; Tollinger et al. 2001; Hill et al. 2000; Skrynnikov et al. 2001) focusing on single-, zero-, double- and multiple-quantum coherences (Dittmer and Bodenhausen 2004; Loria et al. 1999; Tollinger et al. 2001; Korzhnev et al. 2005) as reporters of exchange.

Recently, our laboratories have initiated studies of dynamics in RNA. Here we have made use of the deuteron as a spin-spy probe of motion, using a labeling scheme where all of the ribose carbons are uniformly ^{13}C labeled and all of the ribose hydrogens labeled with ^{2}H, with the exception of the H2′ hydrogen (Vallurupalli et al. 2006; Scott et al. 2000), Fig. 1. A series of $^{1}H \rightarrow {}^{13}C \rightarrow {}^{2}H$ out-and-back experiments have been developed for quantifying ^{2}H spin relaxation (Vallurupalli et al. 2006). This labeling scheme produces an H2′ proton that is isolated from scalar (*J*) couplings to other ribose protons and our goal was to exploit the ''apparent'' $^{1}H2'$–$^{13}C2'$ AX spin system on

P. Vallurupalli · L. E. Kay (✉)
Departments of Medical Genetics, Biochemistry and Chemistry, The University of Toronto, Toronto, ON, Canada M5S 1A8
e-mail: kay@pound.med.utoronto.ca

L. Scott · J. R. Williamson
Departments of Molecular Biology and Chemistry, The Skaggs Institute for Chemical Biology, The Scripps Research Institute, North Torrey Pines Road, La Jolla, CA 92037, USA

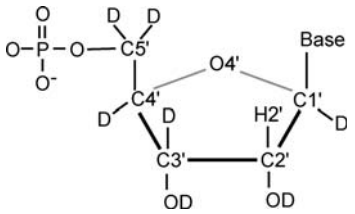

Fig. 1 Labeling scheme used to study both ps-ns (Vallurupalli et al. 2006; Scott et al. 2000) and ms dynamics in ribose units of RNA. All ribose carbons are ^{13}C labeled and all the protons except H2′ are replaced by ^{2}H. In the HIV-2 TAR RNA construct under study (Brodsky and Williamson 1997; Dayie et al. 2002) the C2′ and C3′ carbons can have very similar chemical shifts (74.8–76.8 ppm) and (71.9–77.6 ppm), respectively (Brodsky and Williamson 1997; Dayie et al. 2002), so that strong coupling between the carbons is a distinct possibility in many cases ($^{1}J_{C1'C2'}$~ 40 Hz; 8 C2′–C3′ pairs with $^{1}J_{C1'C2'}/\Delta\nu >$ 0.27, where $\Delta\nu$ is the difference in shifts between C2′ and C3′ at 600 MHz ^{1}H frequency). The C1′ chemical shifts (89.2–94.5 ppm) are well separated from C2′ (Brodsky and Williamson 1997; Dayie et al. 2002)

each of the ribose sugars to record ^{1}H CPMG experiments measuring exchange in RNA. To our initial surprise, however, many more ''dispersions'' were observed than expected in the HIV-2 TAR RNA system studied here, and all of these were artifactual. At the root of the problem is the fact that the C2′ and the adjacent C3′ carbons can have very similar chemical shifts, with differences <1ppm for eight of the 30 nucleotides in HIV-2 TAR (Brodsky and Williamson 1997; Dayie et al. 2002), and since $^{1}J_{C2'C3'} \sim 40$ Hz the two carbons become strongly coupled in cases where the shift differences are small. The strong coupling introduces artifacts in X-pulse CPMG based experiments recorded on heteronuclear ABX spin systems that one might not initially anticipate, and in what follows we provide a theoretical description of the problem, simulations to illustrate how large the effects can be, followed by a simple pulse element that largely suppresses the artifacts.

Results and discussion

We first consider a 3-spin heteronuclear ABX spin-system and evaluate the response of transverse X magnetization to the application of an X-pulse CPMG train. This spin system is sufficient to describe the artifacts that are observed in ^{1}H CPMG relaxation dispersion experiments recorded on RNA samples labeled as in Fig. 1 (Vallurupalli et al. 2006), where spins A and B are ^{13}C2′ and ^{13}C3′, respectively, and spin X is H2′. In what follows we first examine the spin echo pulse element, τ–π_X–τ, that forms the basis of the X-pulse CPMG scheme. The Hamiltonian of interest during the evolution time τ, neglecting both the effects of relaxation and chemical exchange, is given by,

$$H_{ABX} = \omega_A A_Z + \omega_B B_Z + \omega_X X_Z + 2\pi J_{AX} A_Z X_Z + 2\pi J_{AB}(A_X B_X + A_Y B_Y + A_Z B_Z) \quad (1)$$

where ω_A, ω_B and ω_X are the Larmor frequencies of spins A, B and X, respectively, C_J $j\in\{X, Y, Z\}$ is the J-component of the $C\in\{A, B, X\}$ spin-angular momentum operator, J_{AX} is the one bond heteronuclear scalar coupling constant between directly attached spins A and X, J_{AB} is the homonuclear coupling constant connecting spins A and B and we assume that $J_{BX} = 0$. In the case of a heteronuclear AMX spin system where homonuclear spins A and M are only weakly coupled and starting from X_X (proportional to the x-component of X magnetization), the density matrix at the completion of the τ–π_X–τ echo is given by

$$\rho(2\tau) = U_{AMX} X_X U_{AMX}^{-1} \quad (2)$$

where $U_{AMX} = e^{-iH_{AMX}\tau} e^{-i\pi X_X} e^{-iH_{AMX}\tau}$. Since all of the terms comprising the Hamiltonian commute U_{AMX} can be replaced by $e^{-i\pi X_X}$. Thus both chemical shift and scalar coupled evolution during τ are refocused and the starting magnetization is completely recovered. In the case of an ABX system, evolution of X magnetization during the spin echo leads to,

$$\rho(2\tau) = U_o U_{ABX} X_X U_{ABX}^{-1} U_o^{-1} \quad (3.1)$$

where

$$U_o = e^{-iH_o\tau}, \quad (3.2)$$

$$U_{ABX} = e^{-iH^1_{ABX}\tau} e^{-i\pi X_X} e^{-iH^1_{ABX}\tau}, \quad (3.3)$$

$$H^o = \frac{(\omega_A + \omega_B)}{2}(A_Z + B_Z) + 2_{AB} A_Z B_Z \text{ and} \quad (3.4)$$

$$H^1_{ABX} = \frac{(\omega_A - \omega_B)}{2}(A_Z - B_Z) + 2\pi J_{AX} A_Z X_Z + 2\pi J_{AB}(A_X B_X + A_Y B_Y). \quad (3.5)$$

Equation (3.1) can be simplified by noting that $[H^o, H^1{}_{ABX}] = 0$ so that

$$\rho(2\tau) = U^{\text{eff}}_{ABX} X_X U^{\text{eff},-1}_{ABX} \quad (3.6)$$

where

$$U^{\text{eff}}_{ABX} = e^{-iH^1_{ABX}\tau} e^{-iH^2_{ABX}\tau} e^{-i\pi X_X}, \text{ and} \quad (3.7)$$

$$H^2_{ABX} = \frac{(\omega_A - \omega_B)}{2}(A_Z - B_Z) - 2\pi J_{AX} A_Z X_Z + 2\pi J_{AB}(A_X B_X + A_Y B_Y). \quad (3.8)$$

Note that the unitary operator U^{eff}_{ABX} cannot be replaced by $e^{-i\pi X_X}$ in Eq. (3.6) because $[A_X B_X + A_Y B_Y, 2A_Z X_Z] \neq 0$. Thus, X spin magnetization is incompletely refocused after a spin echo in this case. More quantitatively, in the limiting case where $\delta\omega = \omega_A - \omega_B = 0$ and starting from X_X, the fraction of transverse X magnetization at the completion of a single spin echo is given by

$$1 + (J^2_{AB} J^2_{AX}/J^4)\left(8\cos\left(\frac{2\pi J\tau}{2}\right) - 2\cos(2\pi J\tau) - 6\right),$$
$$J^2 = 4J^2_{AB} + J^2_{AX}, \quad (4)$$

and the general case where $\delta\omega \neq 0$ is illustrated in Fig. 2. In the limit that $\delta\omega \gg J_{AB}$ an AMX spin system results and Fig. 2 shows that there is complete refocusing of magnetization, as expected.

The loss of X spin magnetization in the ABX system after a single spin echo can lead to artifacts in CPMG experiments that are comprised of multiple echo trains. In the constant time (CT) variant of the CPMG experiment (Mulder et al. 2001), a series of spin echo elements, $(\tau - \pi_X - \tau)_N$, where N is even, is applied during a constant relaxation delay, $T_{\text{CPMG}} = N \times 2\tau$. The magnitude of the x-component of transverse X magnetization (I) is measured in a series of experiments in which the number of π pulses is varied in the constant time interval. Subsequently, relaxation dispersion curves are generated from the variation of the effective relaxation rate $R_{2,\text{eff}}(\nu_{\text{CPMG}}) = \frac{-1}{T_{\text{CPMG}}} \ln \frac{I(\nu_{\text{CPMG}})}{I_o}$ with ν_{CPMG}, where $\nu_{\text{CPMG}} = \frac{1}{4\tau}$ and I_0 is measured from a reference spectrum with $T_{\text{CPMG}} = 0$. Note that in the absence of chemical exchange and neglecting spin relaxation $R_{2,\text{eff}}(\nu_{\text{CPMG}})$ profiles are expected to be flat since $I(\nu_{\text{CPMG}})$ should be independent of ν_{CPMG}. However, for an isolated ABX spin system the loss of X-transverse magnetization that can result from A–B strong coupling effects during the T_{CPMG} interval ultimately leads to "spikes" in CPMG dispersion profiles corresponding to elevated $R_{2,\text{eff}}$ values that have nothing do with chemical exchange, Fig. 3A. It is noteworthy that artifacts are also produced using a scheme in which in-phase (X_X) and anti-phase ($2A_Z X_Y$) transverse magnetization are interchanged in the middle of the CPMG element that eliminates contributions to dispersion profiles from differential relaxation of these two modes (Loria et al. 1999), Fig. 3B.

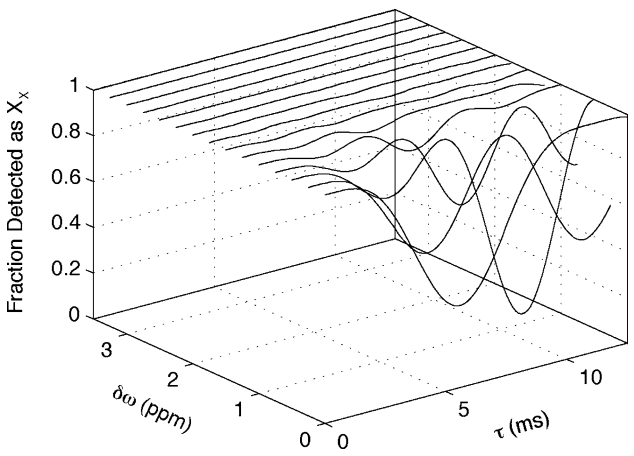

Fig. 2 Fraction of transverse X magnetization, X_X, in a heteronuclear ABX spin system at the completion of a single spin echo, $\tau - \pi_X - \tau$, as a function of τ and $\delta\omega$, the difference in chemical shifts between spins A and B (ppm). The initial magnetization is X_X. A static magnetic field strength of 14.1T (600 MHz ^{1}H frequency and 150 MHz ^{13}C frequency) is assumed along with $X = {}^1\text{H}2'$, $A = {}^{13}\text{C}2'$, $B = {}^{13}\text{C}3'$, $J_{AB} = 40$ Hz, $J_{AX} = 160$ Hz.

Certain aspects of the profiles of Fig. 3A can be understood by comparing the evolution of X-spin transverse magnetization during CPMG elements with very short delays, τ, (large ν_{CPMG}) relative to the evolution for longer values of τ. In the limit that $H^1_{ABX}\,\tau \ll 1$, $H^2_{ABX}\,\tau \ll 1$, the relevant propagator for the evolution of transverse X magnetization, $e^{-iH^1_{ABX}\tau} e^{-iH^2_{ABX}\tau} e^{-i\pi X_X}$ (see above) can be approximated by $e^{-i(H^1_{ABX}+H^2_{ABX})\tau} e^{-i\pi X_X}$; since $[H^1_{ABX} + H^2_{ABX}, X_X] = 0$, X transverse magnetization is preserved. For longer τ values $e^{-iH^1_{ABX}\tau} e^{-iH^2_{ABX}\tau} \neq e^{-i(H^1_{ABX}+H^2_{ABX})\tau}$ and the incomplete refocusing can lead to large $R_{2,\text{eff}}$ rates for certain ν_{CPMG} values. This can be appreciated on an intuitive level by noting that transverse X magnetization, X_X, evolves due to A–X scalar coupling ($2A_Z X_Z$; Eq. (3.5)) to produce $2A_Z X_Y$ which in turn evolves under ($2A_X B_X + 2A_Y B_Y$, Eq. (3.5)) to generate other magnetization modes which are not refocused (see Eq. (3.7)). Thus, a simple solution to the problem becomes apparent: the strong coupling artifacts can be eliminated using the scheme of Fig. 3A if the buildup of anti-phase magnetization, $2A_Z X_Y$, is prevented. Interestingly, in the case where the starting coherence is $2A_Z X_Y$, Fig. 2B, evolution due to strong coupling occurs even in the limit of large ν_{CPMG} values, leading to loss of magnetization and thus non-zero $R_{2,\text{eff}}(\nu_{\text{CPMG}} = \infty)$ rates even though intrinsic relaxation times are assumed infinite in the simulations.

Figure 3C shows that by decoupling spins A and B, and hence preventing the scalar coupled evolution of X_X, artifacts disappear (note the z-axis scale). Here a

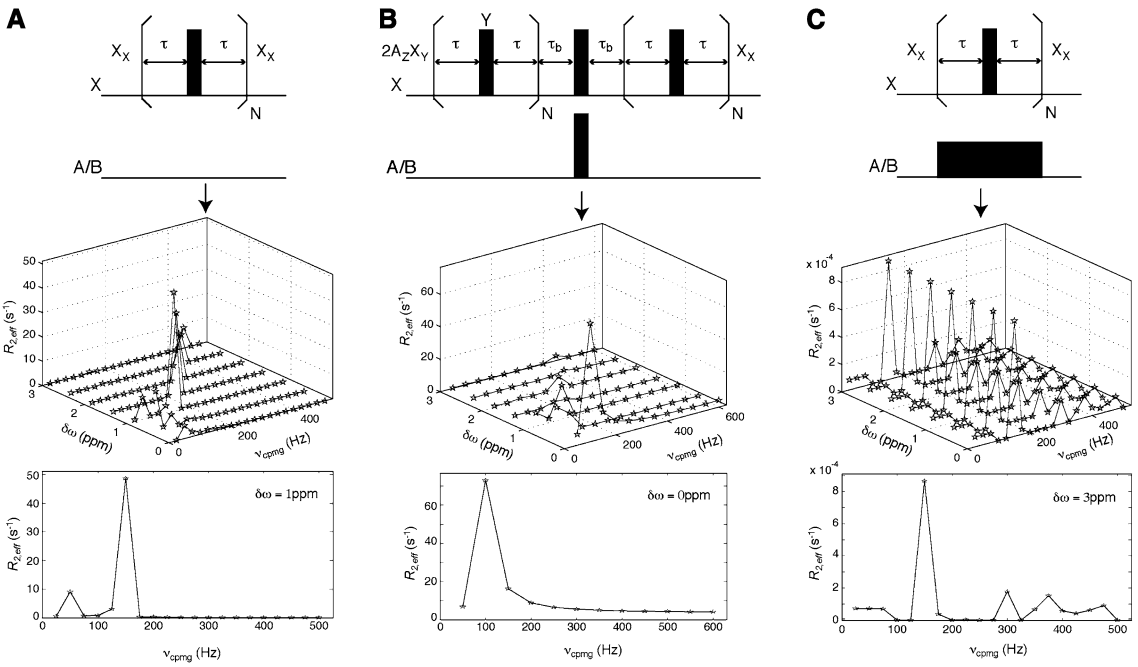

Fig. 3 Constant time X-pulse CPMG schemes along with simulated relaxation dispersion profiles for a heteronuclear ABX spin system with $X = {}^{1}H2'$, $A = {}^{13}C2'$, $B = {}^{13}C3'$, $J_{AB} = 40$ Hz, $J_{AX} = 160$ Hz, as a function of $\delta\omega = \omega_A - \omega_B$. The strength of the CPMG field is given by $\nu_{CPMG} = \frac{1}{4\tau}$, where 2τ is the time between the 180° pulses and RF inhomogeneity is not taken into account. The length of the constant time CPMG element, $T_{CPMG} = 40$ ms, is $2N\tau$ in **A** and **C** and $4N\tau$ in **B**. The starting magnetization is X_X in schemes **A**, **C** and $2A_ZX_Y$ in **B**. The element in the center of the CPMG interval of scheme **B** interchanges $2A_ZX_Y$ and X_X with τ_b set to $1/(4J_{AX})$ (Loria et al. 1999). A CW spin lock field of 100 kHz, on resonance for spin A, has been assumed in **C**. The intrinsic relaxation rates of all spins are set to zero and chemical exchange effects are not included. Highlighted are dispersion curves for particular $\delta\omega$ values for which large artifacts (very high $R_{2,\text{eff}}$ values) were obtained

100 kHz CW field was employed to illustrate the concept and to ensure complete decoupling; such field strengths are, of course, not of any practical interest. When more reasonable fields are used artifacts do result, however, as illustrated in Fig. 4A where a 3 kHz CW field is employed and dispersion profiles simulated as a function of offset from the resonance frequencies of spins A and B that are degenerate. This again can be understood intuitively by noting that a CW field of strength Z kHz can be thought of as a series of 180° pulses (one immediately following the other), each of duration 1/(2Z) ms. If the field strength is such that ''an integer number of such pulses'' can be applied for each τ interval in the CPMG train then A–X scalar coupled evolution is refocused. By contrast, if a half integer number of pulses is applied then the centers of the A/B and X 180° pulses coincide, leading to scalar evolution that for certain T_{CPMG} values produces spikes. Thus, spikes in $R_{2,\text{eff}}$ can be realized for τ values (ms) of {0.5, 1.5, 2.5, 3.5, …./(2Z), although the details do very much depend on T_{CPMG}, and on the parameters of the spin system including couplings and chemical shift offsets, as well as on the offset of the CW field from the spins; indeed spikes can also be obtained for other τ values as well. For example, for a 3 kHz CW field and $T_{CPMG} = 30$ ms considered in Fig. 4A, large artifacts are obtained for ν_{CPMG} values of 200, 333, 433 and 600 Hz, corresponding to τ values that ''accommodate 7.5, 4.5, 3.5 and 2.5 pulses'', respectively. Similar artifacts are observed at ν_{CPMG} values of 200, 333, 429 and 600 Hz even when $J_{AB} = 0$. Thus, it is important to choose the decoupling field strength with care. This can be done by simulating strong coupling effects prior to the experiment and subsequently avoiding ν_{CPMG} values that lead to artifacts. However, the approach that we favor is to vary the CW field strength, ν_{CW}, for each ν_{CPMG} value in such a way so as to ensure that an integral number of decoupling pulses is present in every τ element. This is accomplished by choosing $\nu_{CW} = 2k\nu_{CPMG}$ where k is an integer, Fig. 4B. Flat dispersion profiles are obtained, with the exception of the first point ($\nu_{CPMG} = 33$ Hz) in the case of large $\Delta\omega$ values where the limited bandwidth of the CW field becomes an issue. Thus, dispersion curves can be faithfully recorded in this manner for values of ν_{CPMG} >50 Hz, using CW fields that vary between 2.1 kHz and 3 kHz (see legend to Fig. 4). Detailed simulations with T_{CPMG} values that vary from 20 ms to 100 ms establish that, in general, for ν_{CPMG} >60 Hz, artifacts in $R_{2,\text{eff}}$ are less than 1 s^{-1}. Finally, it is

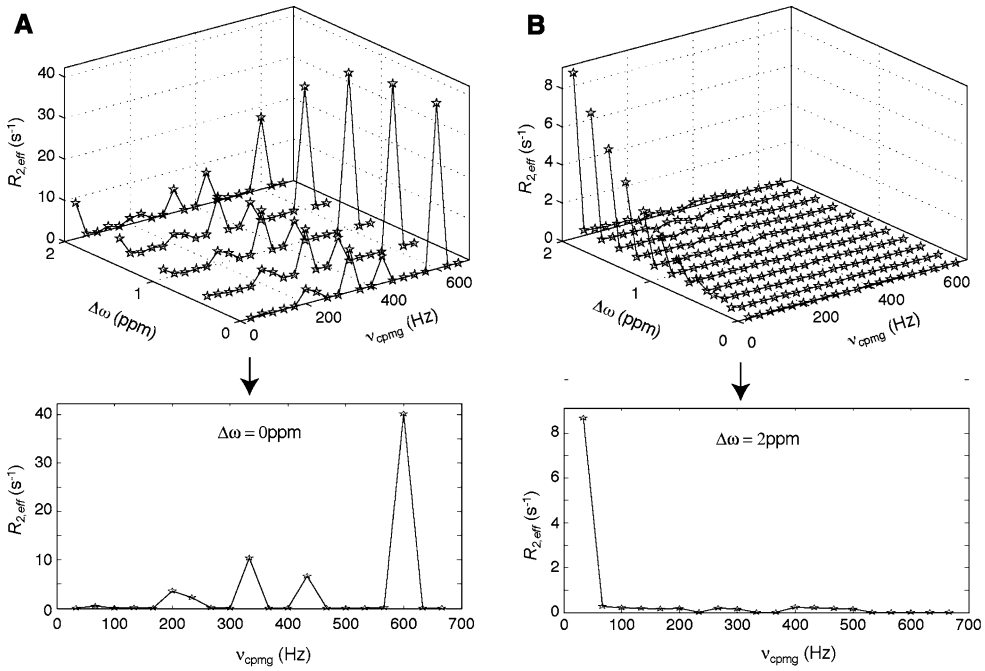

Fig. 4 Relaxation dispersion curves obtained using the pulse sequence of Fig. 3C, with T_{CPMG} = 30 ms, $\delta\omega$ = 0 and $\Delta\omega$ is the offset of C2′/C3′ resonance frequencies from the ^{13}C carrier (see legend to Fig. 3 for additional parameters used in the simulations of the non-exchanging heteronuclear spin system). (**A**) A constant 3 kHz CW field is used for all ν_{CPMG} values, producing large artifacts at a number of frequencies, as described in the text. RF inhomogeneity is not taken into account. (**B**) CW fields are varied with each value of ν_{CPMG}, so as to satisfy $\nu_{CW} = 2k\nu_{CPMG}$, with k an integer, eliminating the artifacts in **A** (ν_{CW} values ranging between 2.1 kHz and 3 kHz are employed). Values of $R_{2,eff}$ larger than 1 s^{-1} are only observed in the first point (ν_{CPMG} = 33.3 Hz) for large $\Delta\omega$ due to the limited bandwidth of the CW field.

straightforward to compensate for the differential heating that may result from this approach by including a short variable A/B spin decoupling element immediately prior to the start of sequence so that the average power dissipated in the sample is independent of ν_{CPMG}.

Figure 5 shows experimental dispersion profiles generated for A35 (A) and G34 (B) of HIV-2 TAR RNA using the schemes of Fig. 3B (green) and 3C (red). The dispersion profiles generated with a standard sequence (Fig. 3B) could easily (and erroneously) be interpreted in terms of exchange, yet clearly reflect the effects of strong coupling. Reasonably flat dispersions are obtained when a CW field satisfying $\nu_{CW} = 2k\nu_{CPMG}$ is applied during the CPMG pulse train, as expected on the basis of the simulations discussed above. A measure of

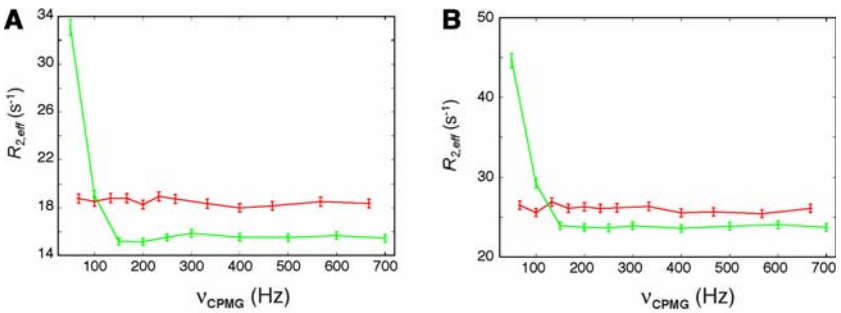

Fig. 5 Comparison of experimental relaxation dispersion curves recorded on a 30 nucleotide, 1 mM HIV-2 TAR RNA sample (Vallurupalli et al. 2006) described previously, 25°C, 600 MHz. The schemes of Fig. 3B (green; T_{CPMG} = 40 ms) and 3C (red; T_{CPMG} = 30 ms) have been used. The CW decoupling field (ν_{CW}) for each ν_{CPMG} value was chosen according to the relation $\nu_{CW} = 2k\nu_{CPMG}$ (with k an integer, as described in the text) and varied between 2.8 kHz and 2.27 kHz. The ^{13}C and ^{1}H carriers were placed at 75.5 ppm and 4.5 ppm, respectively. (**A**) Residue A35 with $|\delta\omega_{C2'C3'}|$ = 0.1 ppm. (**B**) Residue G34, $|\delta\omega_{C2'C3'}|$ = 0.7 ppm

how ''flat'' such dispersions are can be obtained from the quantity RMSD $= \sqrt{\frac{1}{N}\sum_{i=1}^{N}\left(\frac{R_{2,\mathrm{eff},i}^{\mathrm{Exp}} - R_{2,\mathrm{eff},i}^{\mathrm{BestFit}}}{\sigma_{R_{2,\mathrm{eff},i}^{\mathrm{Exp}}}}\right)^2}$, where N is the number of ν_{CPMG} points defining the dispersion, $R_{2,\mathrm{eff},i}^{\mathrm{Exp}}$ is the measured relaxation rate for the ith ν_{CPMG} value, $R_{2,\mathrm{eff},i}^{\mathrm{BestFit}}$ is the value of the horizontal line which best approximates the data and $\sigma_{R_{2,\mathrm{eff},i}^{\mathrm{Exp}}}$ is the error in the measured $R_{2,\mathrm{eff},i}^{\mathrm{Exp}}$ rate. Values of RMSD were 0.9 and 0.6 for A35 and G34, respectively, and varied between 0.5 and 0.9 for the range of strongly coupled residues that could be quantified in spectra.

In summary we have presented an example of where strong coupling effects can lead to substantial artifacts in relaxation dispersion profiles. Dispersion curves generated from ^{1}H CPMG experiments using ^{13}C–^{13}C–^{1}H spin system probes, that are not undergoing chemical exchange but where the pair of ^{13}C spins are strongly coupled, can be produced that are not dissimilar from those that might be obtained in cases with exchange. A simple solution involving the use of CW decoupling fields during the CPMG interval substantially reduces the artifacts so that robust measures of exchange can be obtained.

Acknowledgments PV acknowledges a postdoctoral fellowship from the Canadian Institutes of Health Research Training Grant in Protein Folding and Disease. This research was supported by a grant from the Natural Sciences and Engineering Research Council to LEK. LEK holds a Canada Research Chair in Biochemistry.

References

Bezsonova I, Korzhnev DM, Prosser RS, Forman-Kay JD, Kay LE (2006) Hydration and packing along the folding pathway of SH3 domains by pressure-dependent NMR. Biochemistry 45:4711–4719

Brodsky AS, Williamson JR (1997) Solution structure of the HIV-2 TAR-argininamide complex. J Mol Biol 267:624–639

Dayie KT, Brodsky AS, Williamson JR (2002) Base flexibility in HIV-2 TAR RNA mapped by solution ^{15}N, ^{13}C NMR relaxation. J Mol Biol 317:263–278

Dittmer J, Bodenhausen G (2004) Evidence for slow motion in proteins by multiple refocusing of heteronuclear nitrogen/proton multiple quantum coherences in NMR. J Am Chem Soc 126:1314–1315

Eisenmesser EZ, Millet O, Labeikovsky W, Korzhnev DM, Wolf-Watz M, Bosco DA, Skalicky JJ, Kay LE, Kern D (2005) Intrinsic dynamics of an enzyme underlies catalysis. Nature 438:117–121

Hill RB, Bracken C, Degrado WF, Palmer AG (2000) Molecular motions and protein folding: Characterization of the backbone dynamics and folding equilibrium of α_2D using ^{13}C NMR spin relaxation. J Am Chem Soc 122:11610–11619

Ishima R, Torchia DA (2003) Extending the range of amide proton relaxation dispersion experiments in proteins using a constant-time relaxation-compensated CPMG approach. J Biomol NMR 25:243–248

Ishima R, Wingfield PT, Stahl SJ, Kaufman JD, Torchia DA (1998) Using amide ^{1}H and ^{15}N transverse relaxation to detect millisecond time-scale motions in perdeuterated proteins: Application to HIV-1 protease. J Am Chem Soc 120:10534–10542

Korzhnev DM, Neudecker P, Mittermaier A, Orekhov VY, Kay LE (2005) Multiplesite exchange in proteins studied with a suite of six NMR relaxation dispersion experiments: an application to the folding of a Fyn SH3 domain mutant. J Am Chem Soc 127:15602–15611

Korzhnev DM, Salvatella X, Vendruscolo M, Di Nardo AA, Davidson AR, Dobson CM, Kay LE (2004) Low-populated folding intermediates of Fyn SH3 characterized by relaxation dispersion NMR. Nature 430:586–590

Loria JP, Rance M, Palmer AG (1999) A relaxation-compensated Carr-Purcell-Meiboom-Gill sequence for characterizing chemical exchange by NMR spectroscopy. J Am Chem Soc 121:2331–2332

Mulder FAA, Skrynnikov NR, Hon B, Dahlquist FW, Kay LE (2001) Measurement of slow (μs-ms) time scale dynamics in protein side chains by ^{15}N relaxation dispersion NMR spectroscopy: Application to Asn and Gln residues in a cavity mutant of T4 lysozyme. J Am Chem Soc 123:967–975

Orekhov VY, Korzhnev DM, Kay LE (2004) Double- and zero-quantum NMR relaxation dispersion experiments sampling millisecond time scale dynamics in proteins. J Am Chem Soc 126:1886–1891

Palmer AG 3rd (2004) NMR characterization of the dynamics of biomacromolecules. Chem Rev 104:3623–3640

Scott LG, Tolbert TJ, Williamson JR (2000) Preparation of specifically ^{2}H- and ^{13}C-labeled ribonucleotides. Method Enzymol 317:18–38

Skrynnikov NR, Mulder FA, Hon B, Dahlquist FW, Kay LE (2001) Probing slow time scale dynamics at methyl-containing side chains in proteins by relaxation dispersion NMR measurements: application to methionine residues in a cavity mutant of T4 lysozyme. J Am Chem Soc 123:4556–4566

Tollinger M, Skrynnikov NR, Mulder FA, Forman-Kay JD, Kay LE (2001) Slow dynamics in folded and unfolded states of an SH3 domain. J Am Chem Soc 123:11341–11352

Vallurupalli P, Scott L, Hennig M, Williamson JR, Kay LE (2006) New RNA labeling methods offer dramatic sensitivity enhancements in 2H NMR relaxation spectra. J Am Chem Soc 128:9346–9347